A review on the intermediate polar GKPer

Corral-Santana, J. M.,[a,*] Álvarez-Hernández, A.,[b,c] Torres, M. A. P.[b,c] and Rodríguez-Gil, P.[b,c]

[a]*European Southern Observatory, Alonso de Córdova 3107, Vitacura, Casilla, 19001, Santiago de Chile, Chile*

[b]*Instituto de Astrofísica de Canarias, E-38205 La Laguna, Tenerife, Spain*

[c]*Departamento de Astrofísica, Universidad de La Laguna, E-38206 La Laguna, Tenerife, Spain*

E-mail: jcorral@eso.org

Nova Persei 1901, also known as GK Per, is an intermediate polar and dwarf nova cataclysmic variable discovered on February 1901. It has been extensively studied in various wavelengths for over a century. This review focuses on the main characteristics of the object and highlights the first dynamical mass study published by [1], 120 years after its discovery.
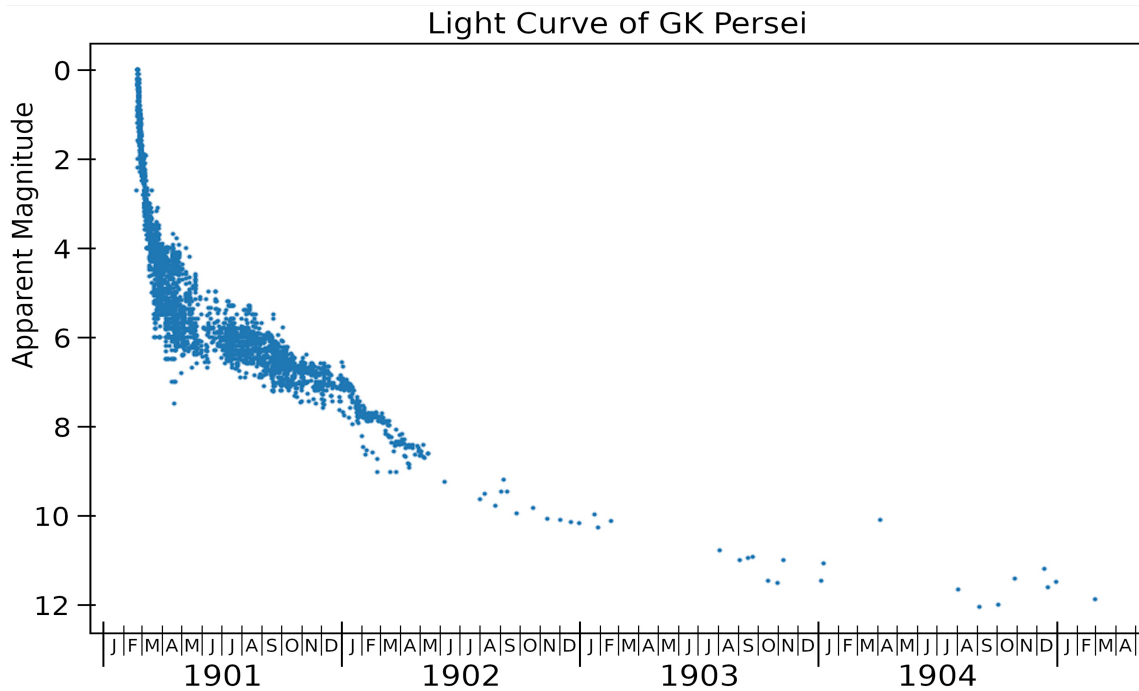
PoS(GOLDEN2023)014

---

*Speaker
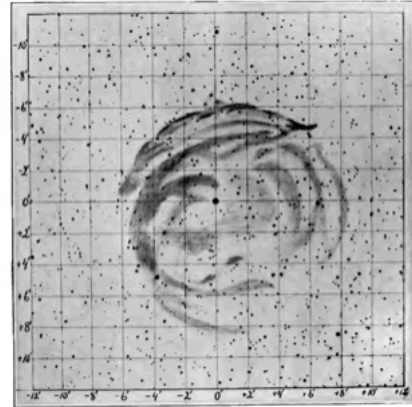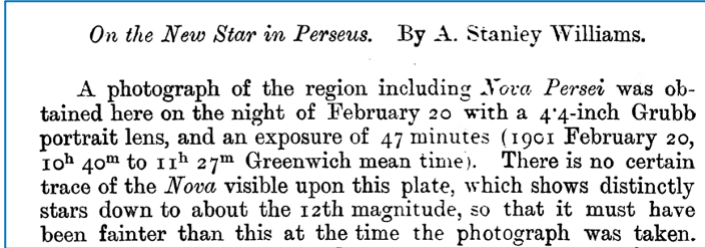
Figure 1: Left: This is the excerpt of the publication by the amateur astronomer Thomas David Anderson in 1901. Taken from [35]. Right: A photographic plate of the GK Per region. An animated version of this image can be found in this link. Image credit: [23].

1. An historical review of GK Per (Nova Persei 1901)

GK Per is a nova that was discovered on February 21st, 1901 by Thomas D. Anderson. Anderson noticed a 3rd magnitude star in the Perseus constellation that had not been there before while walking through the streets of Edinburgh that night. He reported his finding to the Greenwich Observatory. Technical terms are explained when first used, and precise word choice is employed. No new content has been added to the original text. A few days later, Stanley Williams reported his observations from the previous night, February 20th. Despite a 47-minute exposure, he could not find evidence of any nova in the Perseus field with stars down to the 12th magnitude. This means that in slightly more than a day, the 'new' star increased its brightness by more than 9 magnitudes. Figure 1 shows an excerpt of the findings published in [35]. This was the birth of the first new star of the 20th century, named Nova Persei 1901.

Two days after Anderson's discovery, the object reached a visual magnitude of approximately 0.2, which is nearly as bright as Vega. Approximately six days after the explosion, the object's brightness had decreased to visual magnitude 2, and two weeks later, it reached visual magnitude 4. After a few months, the object was no longer visible to the naked eye. Figure 2 illustrates the brightness evolution during the first 3 years, as compiled by the American Association of Variable Star Observers (AAVSO), demonstrating the source's decline to magnitude 12. However, it did not return to its pre-outburst state (visual magnitude ∼ 13 according to William's report) until 11 years after the explosion, in the 1920s, when it was included in the AAVSO's regular observing program. Since the late 1940s, GK Per has remained in what can be called a quiescent state [14] with a relatively stable brightness around visual magnitude 13, showing irregular fluctuations between 12.5 and 13.5 magnitudes. However, in mid-1966, the behaviour of Nova Persei (now known as GK Per) changed, exhibiting periodic increases in brightness up to 11 magnitudes. Since then, it has displayed dwarf nova-like outbursts, with changes in brightness of about 3 magnitudes occurring approximately every 3 years. This is evident in the long-term light curve shown in Figure 3, which was created with the invaluable contributions of amateur astronomers who have observed and monitored the evolution of GK Per over several decades.

Figure 2: Evolution of the Nova Persei explosion between 1901 and 1904. Image credit: Pope Pompous / AAVSO.
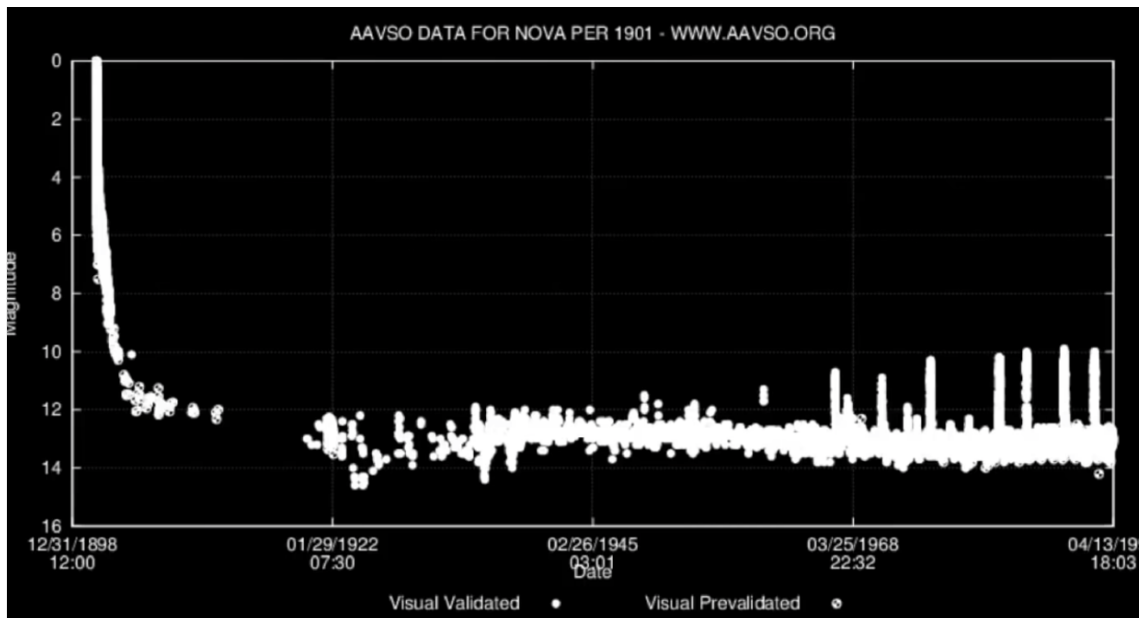
Figure 3: Long-term evolution between 1901 and 1970. Image created with data provided by the AAVSO.

But the outburst has become more extensive and intense over the past five decades. The frequency of outbursts has varied from 385 days around $1948-1967$ to more than 800 days nowadays, as shown by [24]. A possible explanation for this change in outburst frequency could be a decrease in irradiation of the disk produced by the white dwarf over the decades, accompanied by a decrease in viscosity. The study analysed the geometrical, kinematic, and physical properties of the nova shell in GK Per and its interaction with its surroundings at different frequencies [2, 17, 25, 26] and references therein. Far-infrared observations revealed that the nova shell is embedded in an ancient, possibly bipolar planetary nebula centred on the binary and extending approximately ~ 17 arcmin to the north-west and south-east [6]. Upon its discovery, this nebula was initially believed to be the remnant of the binary common envelope phase [3]. However, it has been proposed that the ejecta from the white dwarf progenitor star, expelled during a second asymptotic giant branch phase (and thus a second common envelope event), triggered by a period of high mass transfer rate from the donor star ($> 3 \times 10^{-7}$ M$_\odot$ yr$^{-1} = 1.9 \times 10^{19}$ g s^{-1}), is a more likely origin for the nebula [6]. Figure 5 displays the bipolar planetary nebula, as well as a jet-like structure reported by [27]. According to [17], the knots in the shell expand with velocities ranging from $600-1000$ km/s, with a modest deceleration over time. This can be observed in their figure 3, and an animated version can be found at this link.

In terms of the dynamical characteristics of GK Per, [5] reported a binary orbital period of almost 2 days. [34] confirmed the intermediate polar (IP) nature of GK Per by discovering a WD spin period of 351 s in the modulation of the hard X-ray emission. The U-band flux [21] and the equivalent width of the emission lines at optical wavelengths [10, 22] are also modulated by the spin period.

J-band circular polarimetry of GK Per in quiescence yielded a null detection [29]. However, X-ray spectral modelling estimated the intensity of the WD magnetic field at B$\sim 10^5$ G [33]. The precise dynamical masses of the two stars in GK Per have never been determined due to the largely unconstrained orbital inclination. Eclipses are absent in the light curves, at optical wavelengths, so it has been suggested that the inclination is $i < 73°$ [22]. This, in turn, translates to lower limits on the masses of the white dwarf, M_1, and the donor star M_2.

Different authors have obtained varying values based on optical data: $M_1 > 0.87 \pm 0.24 M_\odot$ [19], $M_1 = 1.15 \pm 0.05 M_\odot$ [11] or $M_1 = 1.22 \pm 0.10 M_\odot$ [28]. On the other hand, estimates of the white dwarf (WD) mass have been proposed, ranging from $M_1 = 0.52^{+0.34}_{-0.16}$ to $M_1 = 1.24 \pm 0.10 M_\odot$, based on the modelling of X-ray spectra.

From an observational perspective, obtaining proper phase coverage of the orbit is difficult due to the nearly to 2-day orbital period (P_{orb}). Only a small range in phase can be observed from a given location. Therefore, [1] concluded that multisite optical observations were the optimal strategy to obtain the complete ellipsoidal modulation. This approach was implemented in [1] and the main findings are summarised in the following section.

2. The first and latest dynamical mass study - 120 years after the nova explosion

In order to maximize the observation coverage of the source, [1] collected photometry and spectroscopy data from various locations around the world. The log of their observations can be found in Table 1. By analysing the donor absorption lines and cross-correlating each GK Per
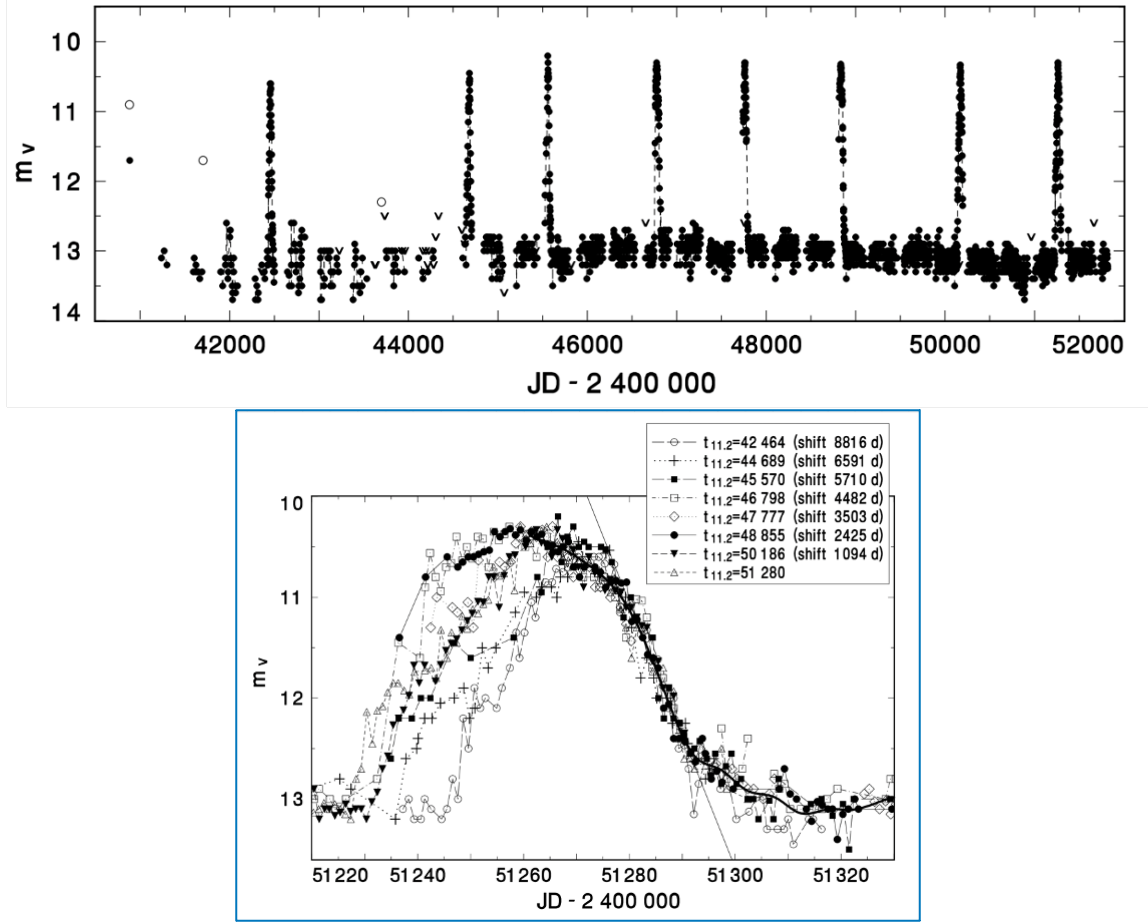
Figure 4: Changes in the recurrent outbursts shown by GK Per in the last decades. Taken from [24].

spectrum with stellar templates, specifically HD 20165 (K1 V) and HR 2556 (K0 III-IV), tbey obtained the orbital parameters. These are shown in Table 2 and were obtained by fitting the radial velocity curve.

Upon comparing their findings with previous results published in the literature, the orbital period derived by [1] agrees within 1-σ with the one reported by [19]. In addition, the K_2 determination of [1] agrees within 1-σ with the value reported by [5] ($K_2 = 124 \pm 2\,\mathrm{km\,s^{-1}}$), but only consistent with the one obtained by [19] ($K_2 = 120.5 \pm 0.7\,\mathrm{km\,s^{-1}}$) at the 4-$\sigma$ level. It is worth noting that [19] also obtained a value of $K_2 = 129 \pm 3\,\mathrm{km\,s^{-1}}$ by combining the radial velocities measured by [16], [5], and [22] without including their own values. The K_2 value mentioned here is consistent with the one presented in [1] at the 1-σ level. Regarding the systemic velocity (γ), [5] and [19] obtained 28 ± 1 and $40.8 \pm 0.7\,\mathrm{km\,s^{-1}}$, respectively. The best-fit value for $\gamma \simeq 32\,\mathrm{km\,s^{-1}}$ given by [1] falls between those two values.

To determine the spectral type of the donor star, [1] utilised two distinct sets of high-resolution spectral templates from [36]: one for main-sequence stars and another for subgiant stars. After adjusting the GK Per spectra accordingly, they found that the best fit corresponds to either a K1 V star with an effective temperature of $T_{eff} = 5198 \pm 60\,\mathrm{K}$ or a supergiant star with $T_{eff} \sim 5000 \pm 60\,\mathrm{K}$
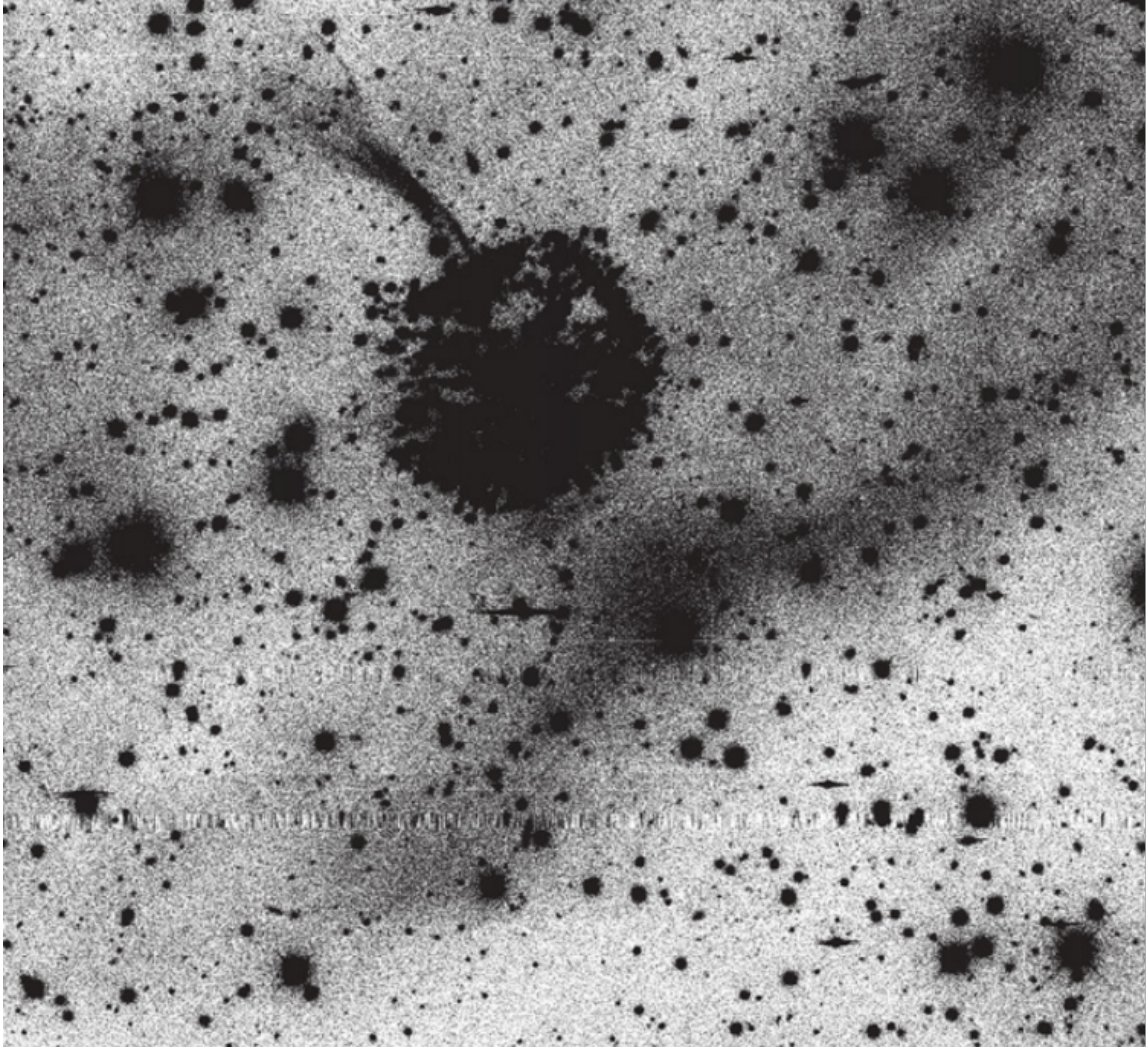
Figure 5: HST image of the area around GK Per. A bipolar-shape nebula is seen surrounding the shell where the nova is embedded. A jet-like structure is also visible. Adapted from [27].

(see [1] for further details). For comparison, previous studies [13] and [12] have also reported a temperature of the donor star $T_2 \sim 5000 \pm 110$ K, which is consistent with their findings.

The rotational velocity of the donor star was then obtained by [1] from the spectra. It was measured in their different spectroscopic datasets using the optimal subtraction technique [18], estimating the uncertainty in the measurements with a Monte Carlo approach (see Álvarez-Hernández et al. 1 for further details). Their sampling was insufficient to establish the phase dependence of $v_{rot} \sin i$, but they covered critical orbital phases to estimate its mean value. They finally derived $v_{rot} \sin i = 52 \pm 2$ km s^{-1}, which corresponds to the mean of the phase-averaged values obtained with both templates, HD 20165 (K1 V) and HR 2556 (K0 III-IV). This value agrees with $v_{rot} \sin i = 55 \pm 10$ km s^{-1} derived by [13] and also (within errors) with $v_{rot} \sin i = 62 \pm 12$, km s^{-1} obtained by [19].

Date	Telescopes	Location	Type of observation
2017 Dec 1	0.4-m robotic	Athens/Greece	Photometry
2017 Dec 6	HCT/HFOSC	Saraswati Mount/India	Spectroscopy
2017 Dec 7	HCT/HFOSC	Saraswati Mount/India	Spectroscopy
	1.3-m JCBT	Tamilnadu/India	Photometry
2017 Dec 8	HCT/HFOSC	Saraswati Mount/India	Spectroscopy
	NOT/ALFOSC	Canary Is./Spain	Spectroscopy
	1.3-m JCBT	Tamilnadu/India	Photometry
	0.4-m robotic	Athens/Greece	Photometry
2017 Dec 9−10	NOT/ALFOSC	Canary Is./Spain	Spectroscopy
	1.3-m JCBT	Tamilnadu/India	Photometry
	0.4-m robotic	Athens/Greece	Photometry
2017 Dec 11	0.4-m robotic	Athens/Greece	Photometry
2018 Jan 21	0.3-m SC30	California/USA	Photometry
2018 Jan 25−26	0.43-m CDK	California/USA	Photometry
2018 Jan 27	0.4-m robotic	Athens/Greece	Photometry
	0.43-m CDK	California/USA	Photometry
2018 Jan 28	0.4-m robotic	Athens/Greece	Photometry
	0.3-m SC30	California/USA	Photometry
	0.43-m CDK	California/USA	Photometry
2018 Jan 29	0.4-m robotic	Athens/Greece	Photometry
2018 Jan 30	0.4-m robotic	Athens/Greece	Photometry
	0.43-m CDK	California/USA	Photometry
2018 Jan 31	0.4-m robotic	Athens/Greece	Photometry
2018 Feb 01−03	0.43-m CDK	California/USA	Photometry
2018 Dec 1	WHT/ISIS	Canary Is./Spain	Spectroscopy
2019 Aug 24−25	WHT/ISIS	Canary Is./Spain	Spectroscopy
2019 Sep 7−8	WHT/ISIS	Canary Is./Spain	Spectroscopy
2019 Sep 12−13	WHT/ISIS	Canary Is./Spain	Spectroscopy
2019 Nov 14	Xinglong/BFOSC	Hebei/China	Spectroscopy

Table 1: Log of observations reported in [1], some of them being simultaneous.

Assuming the system has a circular orbit and is synchronized, they derived the binary mass ratio $q = M_2/M_1$ using the relation: $v_{rot} \sin i \simeq 0.49 \, (1 + q) \, q^{2/3} \, K_2 \, [0.6 \, q^{2/3} + \ln(1 + q^{1/3})]^{-1}$, adopting the [7] approximation for the Roche lobe radius. They obtained $q = 0.38 \pm 0.03$, where the error comes from the standard deviation of 10,000 repetitions calculated for random sets taken from the probability distributions of K_2 and q. This value disagrees with the previously reported $q = 0.28 \pm 0.04$ obtained from the quotient of the donor star and the Hβ radial velocity semi-amplitudes [5]. In another study, $q = 0.55 \pm 0.21$ was estimated using the same technique with lower resolution B-band spectra [19]. According to [1] and [19], the discrepancy with the first value is likely due to the use of the Hβ emission line as a tracer of the white dwarf's motion, which may

Stellar template	K_2	P_{orb}
	(km s^{-1})	(km s^{-1})
HD 20165 (K1 V)	126.4 ± 0.9	1.996872 ± 0.000009
HR 2556 (K0 III-IV)	126.9 ± 0.9	1.996874 ± 0.000009

Table 2: Radial velocity and orbital period of GK Per. Adpated from [1]
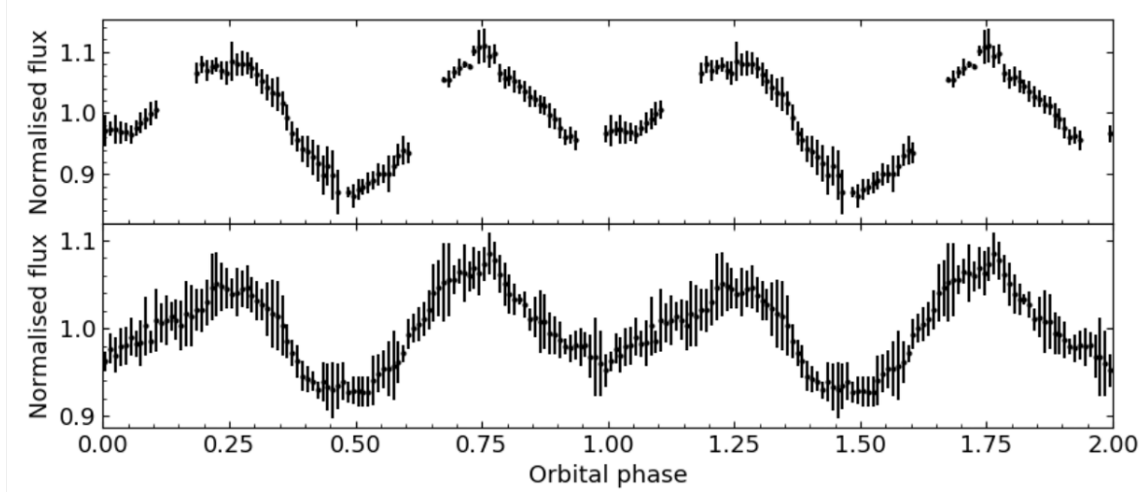
Figure 6: Top: Phase-folded R-band photometry of GK Per considering all data points from all the sites listed in Table 1. Bottom: TESS phase folded photometry of GK Per. Taken from [1].

not be the most reliable indicator. This is especially true considering that GK Per is an IP and its disc is likely truncated due to the intense magnetic field.

Figure 6 (top) displays the R-band light-curve of GK Per obtained by [1], with the photometric observations listed in Table 1. This shows the classical double peak light curve of an ellipsoidal modulation, with minima with different amplitudes at phases 0 and 0.5 but maxima with the same amplitude at phases 0.25 and 0.75. On the other hand, Figure 6bottom shows the light curve obtained by TESS. While the former shows maxima consistent with being identical in amplitude (~ 1.1), the TESS light curve shows hints of unequal maxima at phases 0.25 (with a peak average amplitude ~ 1.04) and phase 0.75 (with a peak average amplitude $\sim 1.08 - 1.1$). This is not so clear in Figure 6 top and it could be related to a disc hot-spot or a spotted donor. To confirm or refute these different maxima in the TESS light curve, multicolour photometry with good coverage of the full orbit is required.

The R-band light curve was modelled by fitting synthetic light curves generated with XRBinary [1]. Developed by E. L. Robinson, this code accounts for the photometric modulation of a binary system. The system is composed of a primary star, assumed to be a point source, surrounded by an accretion disc and a corotating Roche lobe that fully fills the donor star. The input parameters for the study included the inclination i, q, and K_2 as free parameters. A full description of these parameters can be found in section 3.4.2 of [1]. The inclination was allowed to vary between $50 - 85°$ [19, 22],

---

[1]http://www.as.utexas.edu/ēlr/Robinson/XRbinary.pdf

Parameter	Value
P (d)	1.996872 ± 0.000009
K_2 (km s^{-1})	126.4 ± 0.9
$v_{\mathrm{rot}} \sin i$ (km s^{-1})	52 ± 2
q	0.38 ± 0.03
i (°)	67 ± 5
M_1 (M$_\odot$)	$1.03^{+0.16}_{-0.11}$
M_2 (M$_\odot$)	$0.39^{+0.07}_{-0.06}$
R_2 (R$_\odot$)	2.26 ± 0.11

**Figure 7:** Best dynamical parameters of GK Per derived by [1].

while q and K_2 were assigned Gaussian priors with the values listed above. After simulating 10,000 times, the parameters that best fit the model, as derived by [1] are listed in Figure 7 . The best-fitting model light curve is shown in Figure 8 as a solid line.

It is worth noting that the mass derived for the WD ($M_1 = 1.03^{+0.16}_{-0.11}$ M$_\odot$) places it among the more massive ones found in CVs. It is significantly higher than the mean mass of approximately 0.8 M$_\odot$ found by [37] and [20], and it would be one of the ten most massive WDs in Zorotovic's sample.

Figure 9 shows a comparison of the masses obtained through different methods and wavelengths. The dynamical value obtained by [1] presents a good agreement with some previous measurements reported in the literature. In particular, it is quite close to the values derived by [11] and [28] by modelling the optical nova light curve. It also agrees with the mass obtained by [33] using the quiescence-to-outburst Alfvén radius ratio derived from X-ray data. However, the mass estimates coming from X-ray spectra spectral modelling don't show a good agreement with the dynamical value by [1]. In particular, only one of the four values derived from modelling of hard X-ray spectra (which is thought to be much more reliable) presents a $1\,\sigma$ agreement.

Acknowledgement
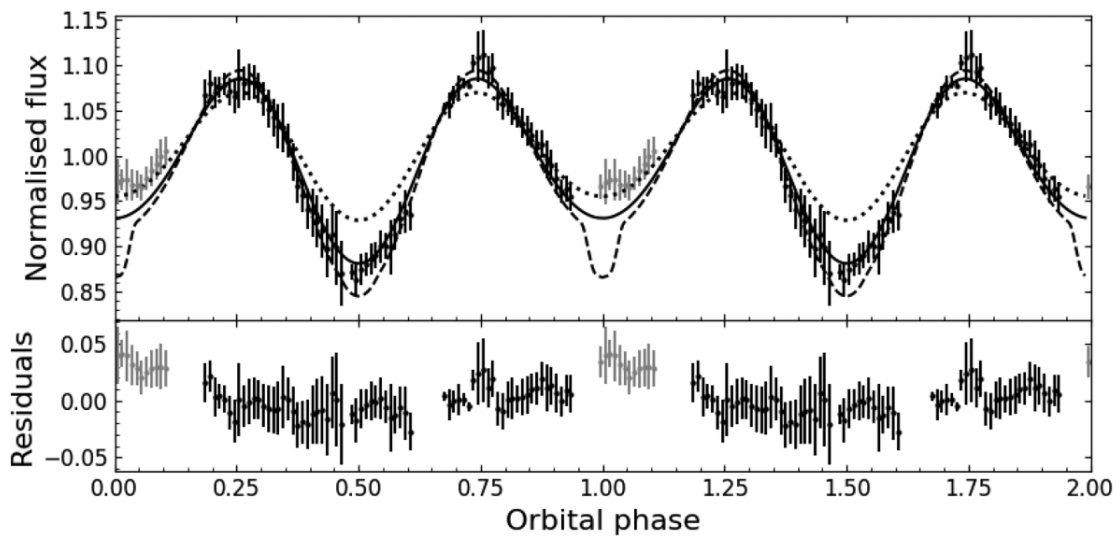
Figure 8: Best-fitting synthetic model (solid line overplotted over the light curve). The dashed line represent the synthetic light curve for $i = 73°$ while the dotted one is for $i = 55°$. Taken from [1].

References

[1] Álvarez-Hernández A., Torres M. A. P., Rodríguez-Gil P., Shahbaz T., Anupama G. C., Gazeas K. D., Pavana M., et al., 2021, MNRAS, 507, 5805. doi:10.1093/mnras/stab2547

[2] Anupama G. C., Kantharia N. G., 2005, A&A, 435, 167. doi:10.1051/0004-6361:20042371

[3] Bode M. F., Seaquist E. R., Frail D. A., Roberts J. A., Whittet D. C. B., Evans A., Albinson J. S., 1987, Natur, 329, 519. doi:10.1038/329519a0

[4] Brunschweiger J., Greiner J., Ajello M., Osborne J., 2009, A&A, 496, 121. doi:10.1051/0004-6361/200811285

[5] Crampton D., Cowley A. P., Fisher W. A., 1986, ApJ, 300, 788. doi:10.1086/163856

[6] Dougherty S. M., Waters L. B. F. M., Bode M. F., Lloyd H. M., Kester D. J. M., Bontekoe T. R., 1996, A&A, 306, 547

[7] Eggleton P. P., 1983, ApJ, 268, 368. doi:10.1086/160960

[8] Evans P. A., Hellier C., 2007, ApJ, 663, 1277. doi:10.1086/518552

[9] Ezuka H., Ishida M., 1999, ApJS, 120, 277. doi:10.1086/313181

[10] Garlick M. A., Mittaz J. P. D., Rosen S. R., Mason K. O., 1994, MNRAS, 269, 517. doi:10.1093/mnras/269.2.517

[11] Hachisu I., Kato M., 2007, ApJ, 662, 552. doi:10.1086/517600

[12] Harrison T. E., 2016, ApJ, 833, 14. doi:10.3847/0004-637X/833/1/14
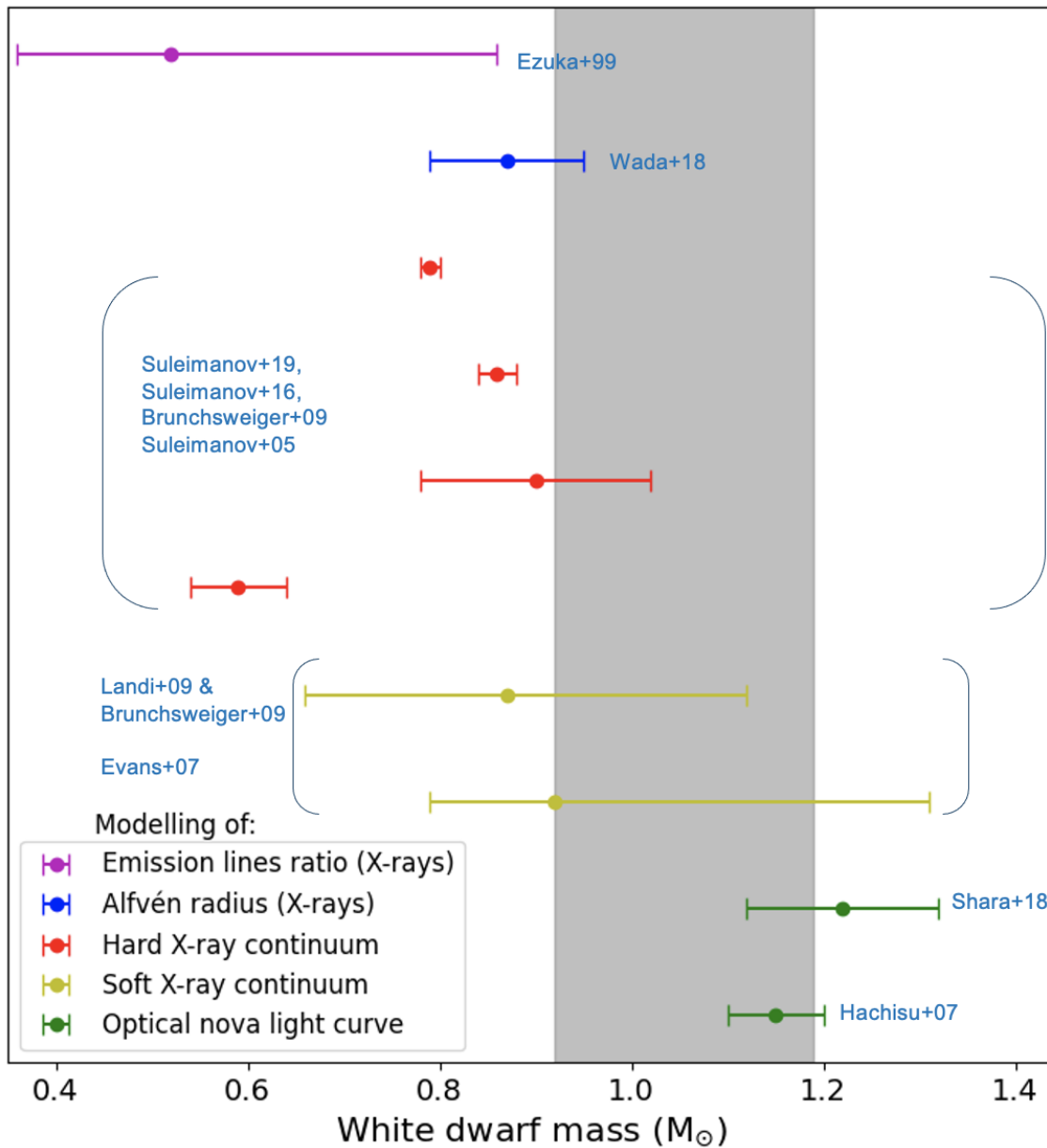
Figure 9: Comparison of GK Per's WD mass obtained through different methods and wavelengths. The gray vertical bar represents the mass and uncertainty derived by [1]. From top to bottom, the estimates obtained by [9] from X-ray emission line ratio; [33] derived from the X-ray Alfvén radius; [4],[30] and [8] from the soft X-ray continuum[4],[31] and [32] from the hard X-ray continuum, and [28] and [11] from the optical light-curve.

[13] Harrison T. E., Hamilton R. T., 2015, AJ, 150, 142. doi:10.1088/0004-6256/150/5/142

[14] Hudec R., 1981, BAICz, 32, 93

[15] Kepler S. O., Pelisoli I., Koester D., Ourique G., Romero A. D., Reindl N., Kleinman S. J., et al., 2016, MNRAS, 455, 3413. doi:10.1093/mnras/stv2526

[16] Kraft R. P., 1964, ApJ, 139, 457. doi:10.1086/147776

[17] Liimets T., Corradi R. L. M., Santander-García M., Villaver E., Rodríguez-Gil P., Verro K., Kolka I., 2012, ApJ, 761, 34. doi:10.1088/0004-637X/761/1/34

[18] Marsh T. R., Robinson E. L., Wood J. H., 1994, MNRAS, 266, 137. doi:10.1093/mnras/266.1.137

[19] Morales-Rueda L., Still M. D., Roche P., Wood J. H., Lockley J. J., 2002, MNRAS, 329, 597. doi:10.1046/j.1365-8711.2002.05013.x

[20] Pala A. F., Gänsicke B. T., Belloni D., Parsons S. G., Marsh T. R., Schreiber M. R., Breedt E., et al., 2022, MNRAS, 510, 6110. doi:10.1093/mnras/stab3449

[21] Patterson J., 1991, PASP, 103, 1149. doi:10.1086/132935

[22] Reinsch K., 1994, A&A, 281, 108

[23] Ritchey G. W., 1901, ApJ, 14, 293. doi:10.1086/140868

[24] Šimon V., 2002, A&A, 382, 910. doi:10.1051/0004-6361:20011560

[25] Seaquist E. R., Bode M. F., Frail D. A., Roberts J. A., Evans A., Albinson J. S., 1989, ApJ, 344, 805. doi:10.1086/167846

[26] Scott A. D., Rawlings J. M. C., Evans A., 1994, MNRAS, 269, 707. doi:10.1093/mnras/269.3.707

[27] Shara M. M., Zurek D., De Marco O., Mizusawa T., Williams R., Livio M., 2012, AJ, 143, 143. doi:10.1088/0004-6256/143/6/143

[28] Shara M. M., Prialnik D., Hillman Y., Kovetz A., 2018, ApJ, 860, 110. doi:10.3847/1538-4357/aabfbd

[29] Stockman H. S., Schmidt G. D., Berriman G., Liebert J., Moore R. L., Wickramasinghe D. T., 1992, ApJ, 401, 628. doi:10.1086/172091

[30] Suleimanov V., Revnivtsev M., Ritter H., 2005, A&A, 435, 191. doi:10.1051/0004-6361:20041283

[31] Suleimanov V., Doroshenko V., Ducci L., Zhukov G. V., Werner K., 2016, A&A, 591, A35. doi:10.1051/0004-6361/201628301

[32] Suleimanov V. F., Doroshenko V., Werner K., 2019, MNRAS, 482, 3622. doi:10.1093/mnras/sty2952

[33] Wada Y., Yuasa T., Nakazawa K., Makishima K., Hayashi T., Ishida M., 2018, MNRAS, 474, 1564. doi:10.1093/mnras/stx2880

[34] Watson M. G., King A. R., Osborne J., 1985, MNRAS, 212, 917. doi:10.1093/mnras/212.4.917

PoS(GOLDEN2023)014

[35] Williams A. S., 1901, MNRAS, 61, 337. doi:10.1093/mnras/61.5.337

[36] Yee S. W., Petigura E. A., von Braun K., 2017, ApJ, 836, 77. doi:10.3847/1538-4357/836/1/77

[37] Zorotovic M., Schreiber M. R., Gänsicke B. T., 2011, A&A, 536, A42. doi:10.1051/0004-6361/201116626

DISCUSSION

MICHAEL SHARA: Can you guess what is the origin of the jet-like structure in GK Per?

JESUS CORRAL-SANTANA: It is not clear but you mentioned me during this workshop that you have found some interesting clues, and you are in the process of publishing the findings. I will keep the secret until then.

   ...

ANTONIO RODRÍGUEZ: You mentioned that the Hβ line is not a good tracer for the WD mass. Can you explain why?

JESUS CORRAL-SANTANA: Using an emission line coming from the disc to trace derive the mass of the compact object is always risky. Only the wings of the line can be used to infer the compact object. However, fitting the wings is very sensitive to e.g. the Gaussian used. In this in particular, GK Per is an intermediate polar which means that the inner disc is truncated at some point due to the strong magnetic field. Hence, at most the wings of the emission line is tracing the innermost orbit before the disc disappears.